Received 19 June 2025; Accepted 9 September 2025
https://doi.org/10.48612/letters/2025-4-249-255
https://elibrary.ru/pijvqm

Evaluation of hardening mechanisms of iron-doped Ti4Al3V alloy obtained using dual-wire electron beam additive manufacturing

A. V. Nikolaeva[†], A. V. Vorontsov, A. O. Panfilov, S. Yu. Tarasov

[†]nikolaeva@ispms.ru

Institute of Strength Physics and Materials Science SB RAS, Tomsk 634055, Russia

Abstract: In this work, the evolution of the grain structure, phase composition, and mechanical properties of the Ti4Al3V alloy additionally alloyed with iron in concentrations ranging from 1.0 to 8.0 wt.%, and manufactured by dual-wire electron beam additive manufacturing (WEBAM) was investigated. A quantitative analysis of the contributions of various strengthening mechanisms to the overall strengthening of the iron-added Ti4Al3V alloy was conducted. It was found that in the range of iron concentrations from 1.0 to 3.0 wt.%, the main strengthening mechanism is grain boundary strengthening (≈59%) due to a decrease in the average size of prior β-Ti grains (from 580 to 470 μm) and the thickness of α-phase lath (from 0.61 to 0.36 μm). The contribution of grain boundary strengthening to the yield strength of the Ti4Al3V-7.5Fe alloy is only 19%. This is due to a reduction in the number of grain boundaries resulting from the transformation of β-Ti grains into a β/ω composite structure. The obtained results enable us to determine the concentration ranges of iron in the Ti4Al3V alloy at which the respective strengthening mechanisms make the greatest contribution to its mechanical properties. Consequently, the presented approaches and models can be employed to optimize both the composition and processing parameters of titanium alloys alloyed with varying iron contents.

Keywords: Ti4Al3V-Fe, electron beam additive manufacturing, mechanical properties, yield strength, hardening mechanisms

Acknowledgments: *The investigations have been carried out using the equipment of Share Use Centre "Nanotech" of the ISPMS SB RAS. The work was performed according to the Government research assignment for ISPMS SB RAS, project FWRW-2024-0001.*

1. Introduction

Additive manufacturing is widely used in the aerospace industry to produce titanium alloy components such as balloons, fan blades, and compressor parts [1–3]. A key drawback is the formation of coarse columnar β-Ti grains due to epitaxial growth, leading to anisotropy and reduced mechanical performance after the β→α+β transformation [4].

Since the mechanical properties of two-phase titanium alloys depend on the post-transformation microstructure, a major challenge is to promote fine, equiaxed β-Ti grains during deposition. This can be addressed by introducing inoculants (e.g., La_2O_3, ZrN, TiN, B, Nb) and alloying with elements like Cr, Si, Ni, Fe, and Cu to enhance constitutional supercooling [5–7].

Study [8] showed that adding 0.1 wt.% Si to Ti6Al4V produced by WAAM refines prior β-Ti grains to 1.5–3.0 mm and reduces α-lath width, increasing strength by over 100 MPa and reducing elongation anisotropy. Strengthening is primarily due to grain boundary and solid solution mechanisms, confirming the beneficial effect of Si on mechanical properties.

According to [9] adding 2.5 vol.% TiB to Ti6Al4V via LDED refines the β-Ti grains (≈200 to ≈70 μm), reduces the α-Ti aspect ratio (≈16.3 to ≈4.8), and promotes the transition from columnar to equiaxed structure. The resulting composite shows a good balance of strength (1153 MPa) and ductility (6.2%). The increase in yield strength is mainly due to strengthening of grain boundaries (45 MPa), dislocations (33 MPa), and mesh structure (54 MPa). TiB particles also enhance strength via the Orowan mechanism (29 MPa). Increasing TiB to 5 vol.% slightly raises strength but reduces ductility due to cracking.

In [10], the effect of Fe alloying on titanium produced by LMD is examined. Adding 2–4 wt.% Fe reduced the grain size from 320 to 220 μm. While Ti-2Fe showed lower strength (UTS 792 MPa, YS 680 MPa), Ti-4Fe improved the strength to 880 MPa and 798 MPa, respectively. In Ti6Al4V-2Fe, grain boundary strengthening (≈64 MPa) dominates, whereas in Ti6Al4V-4.4Fe, solid solution strengthening (≈54 MPa) prevails due to the dissolution of Fe in the β-phase.

Alloying titanium with various elements enhances strength via grain boundary, solid solution, dispersion, and dislocation mechanisms, contributions of which depend on alloying concentration. This study presents a quantitative approach to assess yield strength in Ti4Al3V-Fe alloys and analyze the role of each mechanism.

The aim of this work was to evaluate the contributions of various strengthening mechanisms to the increase in the yield strength of the Ti4Al3V alloy doped with iron in the concentration range of 1.0–8.0 wt.%.

2. Materials and experimental methods

Additive samples in the form of vertical walls were obtained by electron beam additive manufacturing in ISPMS SB RAS from Ti4Al3V titanium alloy doped with 1.0 – 8.0 wt.% iron by simultaneously feeding 1.6 mm Ti4Al3V wire with reduced Al and V contents and 0.8 mm ER70S-6 copper-coated Fe wire. Deposition was carried out on a Grade 2 titanium substrate fixed to a triaxial water-cooled table inside a vacuum chamber. The initial deposition layers were carried out at an accelerating voltage of 30 kV and a beam current of 60 mA. The current was then reduced to 40 mA for Ti4Al3V-1.7Fe and to 50 mA for both Ti4Al3V-2.5Fe and Ti4Al3V-7.5Fe (Fig. 1c). The scanning speed was maintained at 400 mm/min, and the scanning direction was reversed after each deposited layer. Upon completion, specimens for microstructural and mechanical characterization were sectioned from the fabricated walls using an electrical discharge machine (EDM).

Specifically, titanium alloy samples with nominal iron contents of 1 vol.%, 2 vol.%, and 5 vol.% were obtained, corresponding to actual values of 1.7 wt.%, 2.5 wt.%, and 7.5 wt.%, respectively. Sample preparation included mechanical grinding using SiC sandpaper of various grit sizes, followed by polishing with 1/0 diamond paste and a silicon dioxide suspension. Subsequently, the polished surfaces were chemically etched for 15 seconds using a reagent composed of $4HF + 6HCl + 8HNO_3 + 82\ ml\ H_2O$.

The microstructure of the samples was studied using an Axiovert 200MAT inverted reflected light microscope. The sizes of equiaxed β-Ti grains, as well as the volume fractions of equiaxed and columnar grains, were determined by the intercept method. The microstructural features of the samples were examined using a Thermo Fisher Scientific Apreo S LoVac scanning electron microscope equipped with an energy dispersive spectrometer (EDS). To determine the phase composition and analyze the fine structure of the samples, a JEOL JEM-2100 transmission electron microscope with an energy dispersive analyzer was used.

The dimensions of structural elements and the volume fractions of phases present in the Ti4Al3V-Fe alloy were determined using TEM bright-field images, microdiffraction patterns obtained from selected areas, and dark-field images acquired from reflections of the corresponding phases. Phase identification was performed using standard methods involving analysis of selected area electron diffraction (SAED) patterns based on tabulated crystal lattice parameters. X-ray diffraction analysis was carried out using a DRON-7 diffractometer with $Co_{K\alpha}$ radiation ($\lambda = 0.1789$ nm). For precise separation of diffraction peaks, a DRON-8N diffractometer with $Cu_{K\alpha}$ radiation ($\lambda = 0.15406$ nm), equipped with a Mythen 2R 1D X-ray detector, was employed.

Uniaxial tensile tests were performed using a universal testing machine UTS 110M. For these tests, blade-shaped samples were cut with a gauge section measuring $12 \times 2.5 \times 2$ mm, with the tensile axis oriented along both the Z (wall growth direction) and along the Y (layer deposition direction).

3. Results

The morphology of prior β-Ti grains in the Ti4Al3V alloy doped with 1.7 and 2.5 wt.% Fe is represented by columnar-equiaxed grains (Fig. 1a, c). The addition of 7.5 wt.% Fe to the titanium alloy suppresses the epitaxial growth of prior β-Ti grains and promotes a transition from a columnar-equiaxed structure to a fully equiaxed one (Fig. 1e). Analysis

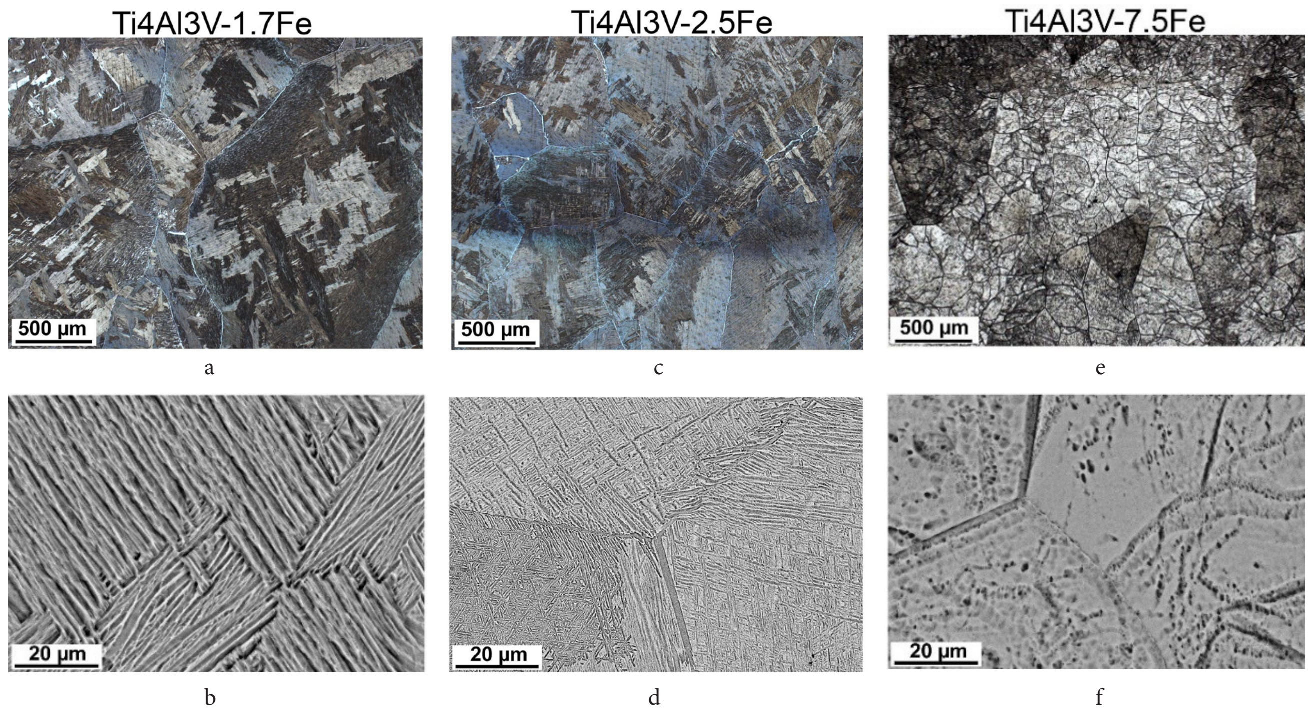

Fig. 1. Macro images and SEM images in the BSE mode of the microstructures of Ti4Al3V-1.7Fe (a, b), Ti4Al3V-2.5Fe (c, d), and Ti4Al3V-7.5Fe (e, f) alloys.

of the scanning electron microscopy data revealed that the microstructures of Ti4Al3V-1.7Fe and Ti4Al3V-2.5Fe alloys consist of α/β-lath colonies and Widmanstätten structures (Fig. 1b, d). Doping with 7.5 wt.% Fe results in full columnar-to-equiaxed transition (CTE) of prior β-Ti grains (Fig. 1f).

The shape of columnar grains in the investigated alloys was evaluated based on the aspect ratio, i.e. ratio between linear intersection length in the growth direction (l) and their intersection width in the perpendicular direction (d), using transversely oriented samples. This aspect ratio, alternatively called the anisotropy coefficient of β-Ti columnar prior grains (l/d), characterizes the degree of grain elongation. With an increase in iron content from 1.7 to 7.5 wt.%, the average size of equiaxed grains in the middle of the alloy cross-section decreases by a factor of 1.5, from 580 ± 65 μm to 390 ± 35 μm. The average anisotropy coefficients of β-Ti columnar grains l/d for Ti4Al3V-1.7Fe, Ti4Al3V-2.5Fe, and Ti4Al3V-7.5Fe alloys are 2.39 ± 0.25, 2.20 ± 0.29, and 1, respectively, which indicates grain refinement and the elimination of columnar structure at the highest iron concentration. It was found that with an increase in the Fe content from 1.7 to 2.5 wt.%, their thickness decreased by a factor of 1.7 (Fig. 1b – d).

Figure 2 shows the results of transmission electron microscopy of Ti4Al3V alloys with different iron contents. Bright-field TEM images (Fig. 2a, e) demonstrate the α/β lath structure for Ti4Al3V-1.7Fe and Ti4Al3V-2.5Fe alloys, which is consistent with the results of scanning electron microscopy (Fig. 1b, d,). Dark-field TEM images acquired under the corresponding reflection conditions (Fig. 2c, d, g, h) enable evaluation of the distribution of α-Ti and β-Ti phases and their morphology. No intermetallic compounds of the Ti-Fe system were found in the alloys with iron contents of 1.7 and 2.5 wt.%.

The bright-field TEM image (Fig. 2i) shows the microstructure characteristic of the Ti4Al3V-7.5Fe alloy. Analysis of the SAED (Fig. 2j) taken from the marked area in Fig. 2i revealed reflections belonging to the ω-Ti phase, which is further demonstrated by the dark-field image acquired under the $(101)_ω$ reflection (Fig. 2k). This indicates the formation of dispersed ω-Ti particles within the β-Ti grains. Despite the high iron content in the Ti4Al3V alloy (7.5 wt.%), no TiFe or Ti_2Fe intermetallic compounds were detected. The average radius of the ω-Ti phase particles ($r_ω$) was determined from the dark-field TEM images to be 4.36 ± 1.22 nm.

The mechanical properties of titanium alloys depend on the size of β-Ti columnar grains (L), the size of equiaxed β-Ti grains (D), and the thickness of α-Ti laths (b), which are used to evaluate the contributions of strengthening mechanisms to the overall strengthening of Ti4Al3V alloy additionally

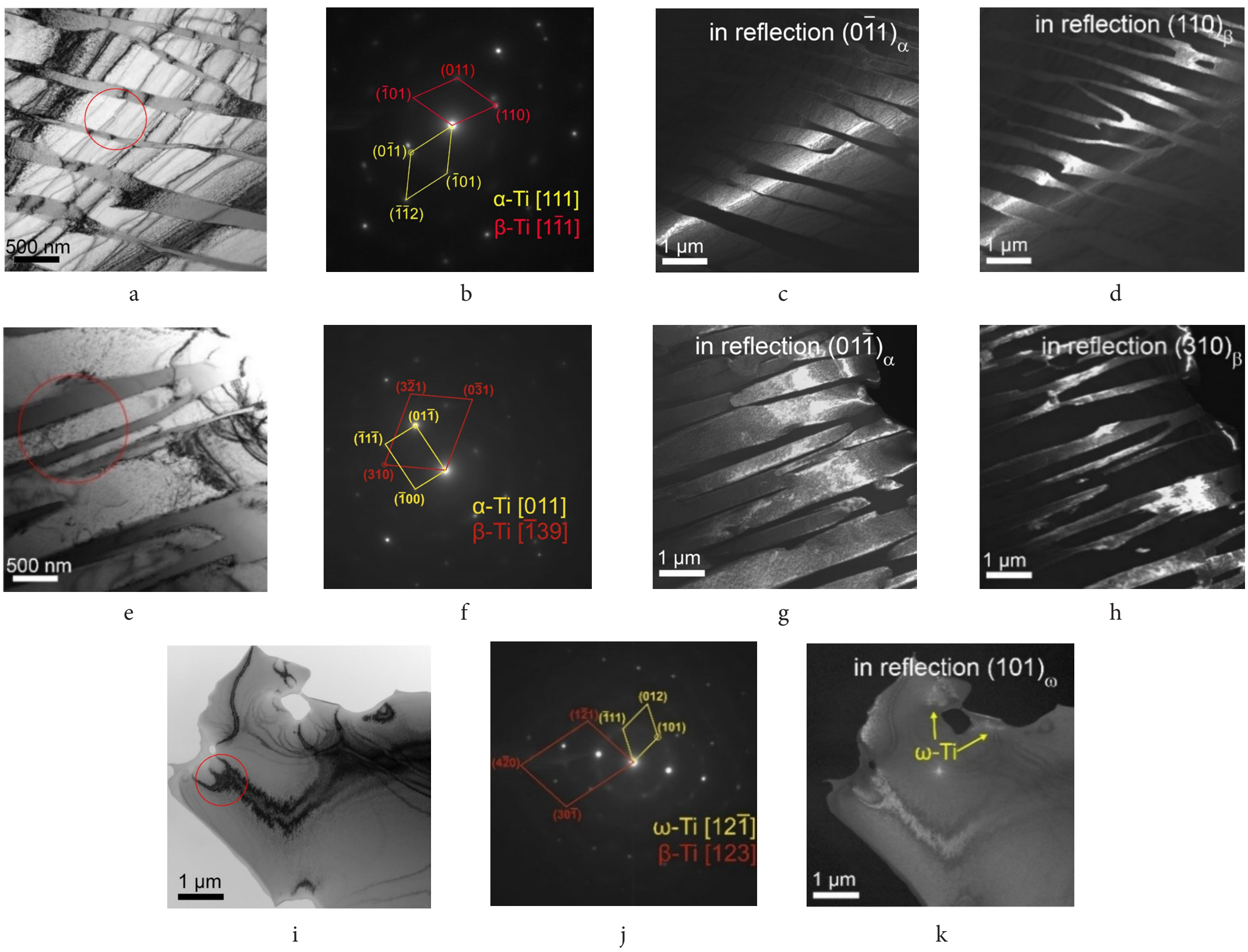

Fig. 2. (Color online) TEM bright-field images of the microstructure of Ti4Al3V alloys with different Fe contents (a, e, i), SAED patterns (b, f, j) obtained from the respective areas (a, e, i), and dark-field images (c, d, g, h, k) acquired under the reflections marked by a closed line in the SAED patterns.

alloyed with iron. The sizes of β-Ti columnar grains were calculated using the Eq. (1):

$$L = 2\sqrt{\frac{l \cdot d \cdot \varepsilon}{\pi}}, \qquad (1)$$

where l is the length of the β-Ti columnar grain along the growth direction, d is the width of the β-Ti columnar grain perpendicular to the growth direction, and ε is a coefficient characterizing the elliptical shape of the columnar grain in the titanium alloy, calculated using the Eq. (2) [11]:

$$\varepsilon = \sqrt{1 - \frac{d^2}{l^2}}. \qquad (2)$$

The average values of these structural characteristics, as well as the volume fractions of columnar $V_{\beta col.}$ and equiaxed β-Ti grains $V_{\beta eq.}$ measured in the middle section of $Ti4Al_3V$-Fe alloys, which is not influenced by the substrate, are presented in Table 1.

According to X-ray diffraction, an increase in the iron content from 1.7 to 7.5 wt.% results in an increase in the intensity of the β-Ti reflections. At the same time, a decrease in the intensity of the α-Ti reflections is observed (Fig. 3). When the Fe content is raised from 1.7 to 7.5 wt.% in Ti4Al3V alloy produced by electron beam additive manufacturing, the volume fraction of the β-Ti precipitates increases from 9% to 92%. Thus, it was established that the middle section of the wall of the Ti4Al3V-7.5Fe alloy consists entirely of prior β-Ti grains.

In the Ti4Al3V-7.5Fe alloy sample, asymmetry is observed in the β-Ti phase X-ray reflections, specifically $(200)_\beta$ and $(211)_\beta$. Since the thermal conditions of the process can promote the formation of metastable phases, the reflections were deconvoluted based on X-ray structural analysis data, which enabled the identification of additional reflections attributed to the isothermal ω-Ti phase, namely $(20\bar{2}1)_\omega$ and $(30\bar{3}0)_\omega$ (Fig. 4 a, b). The volume fraction of the ω-Ti precipitates (f_ω) in the Ti4Al3V-7.5Fe alloy is 3%.

The average values of yield strength, tensile strength, and relative elongation of the Ti4Al3V alloy produced by the WEBAM method are 584 ± 37 MPa, 652 ± 29 MPa, and 0.17, respectively. Figure 5 shows the dependence of the mechanical properties and structural features on the Fe content in the Ti4Al3V alloy. Analysis of these dependencies reveals that increasing the Fe content from 1.7 to 2.5 wt.% results in a decrease in the average size of prior β-Ti grains and the thickness of α-Ti laths, leading to an increase in the

Table 1. Structural characteristics of Ti4Al3V alloy added with various Fe contents.

Alloy	l/d	L, mm	$V_{\beta col.}$, %	D, μm	$V_{\beta eq.}$, %	b, μm
Ti4Al3V-1.7Fe	2.39 ± 0.25	1.61 ± 0.26	88	580 ± 65	12	0.61 ± 0.07
Ti4Al3V-2.5Fe	2.20 ± 0.29	1.09 ± 0.26	75	470 ± 40	25	0.36 ± 0.09
Ti4Al3V-7.5Fe	1	-	0	390 ± 35	100	-

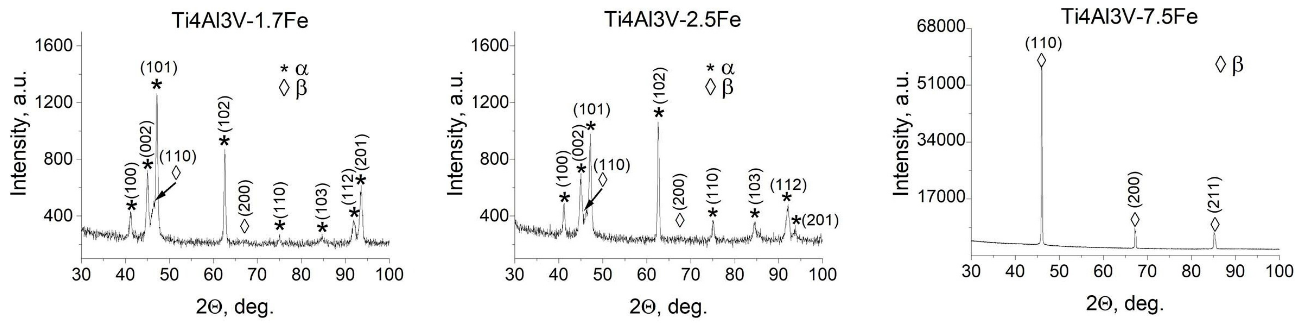

Fig. 3. X-ray diffractograms obtained from the middle part of Ti4Al3V alloy doped with different iron contents.

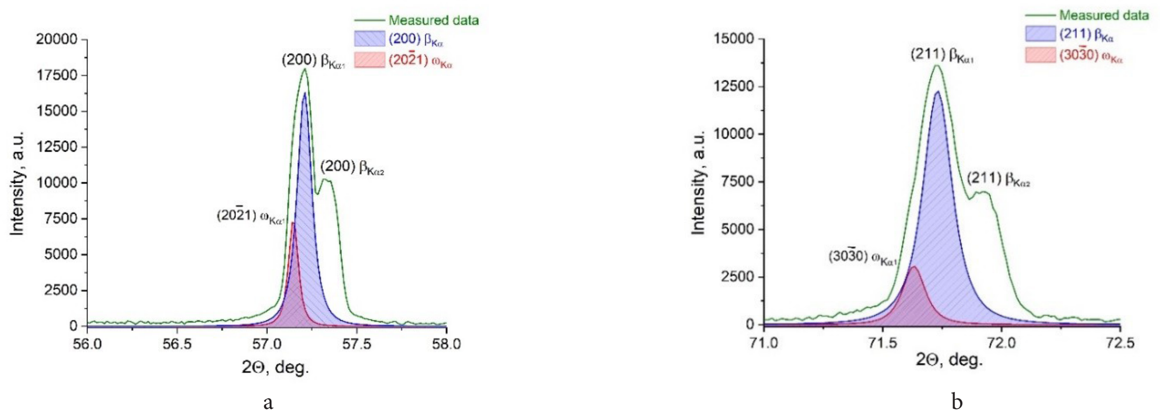

Fig. 4. (Color online) Deconvolution of $(200)_\beta$ (a) and $(211)_\beta$ (b) reflections obtained from X-ray diffraction patterns from the middle part of the Ti4Al3V-7.5Fe wall.

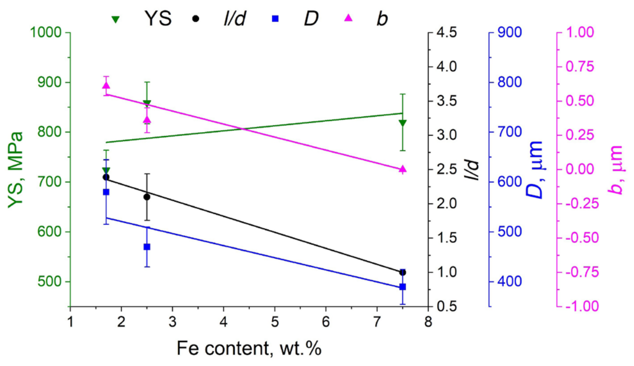

Fig. 5. (Color online) Dependencies of the yield strength (YS), the anisotropy coefficient of the columnar prior grain β-Ti (l/d), the size of equiaxed grains β-Ti (D), thickness of α-Ti laths (b) on the iron content in (Ti-Al-V)+Fe alloys.

yield strength of these alloys by 24% and 40%, respectively, compared to the Ti4Al3V alloy (Fig. 5). The Ti4Al3V alloy doped with 7.5 wt.% Fe exhibits a reduction in yield strength to 820 ± 57 MPa, which is primarily attributed to the formation of the brittle ω-Ti phase.

4. Discussion

The contribution of various strengthening mechanisms to the overall strengthening of the Ti4Al3V alloy, additionally alloyed with iron, was evaluated using a model based on the additive sum of strengthening factors. Within this model, each mechanism is considered to make an independent contribution to the overall increase in the yield strength of the Ti4Al3V alloy. Four main mechanisms are taken into account: grain boundary strengthening, solid solution strengthening, dispersion strengthening, dislocation strengthening and ω-precipitate strengthening. The combined effect of these mechanisms determines the mechanical properties of the Ti4Al3V alloy with iron addition [12,13]:

$$\Delta\sigma_{YS} = \sigma_0 + \Delta\sigma_{GB} + \Delta\sigma_{SS} + \Delta\sigma_{DH} + \Delta\sigma_{DS} + \Delta\sigma_{\omega}, \qquad (3)$$

where σ_{YS} is the calculated value of the alloy's yield strength; σ_0 is the friction stress of dislocations in the α-Ti crystal lattice σ_0 =129 MPa [14]; σ_{GB} is the increase in yield strength due to grain boundary strengthening; σ_{SS} is the increase in yield strength due to solid solution strengthening; σ_{DH} is the increase in yield strength due to dispersion strengthening; σ_{DS} is the increase in yield strength due to dislocation strengthening; σ_{ω} is the ω precipitate strengthening.

It has been established that increasing the iron content in the Ti4Al3V alloy results in a change in the grain structure morphology, involving a full CTE transition. This transition is accompanied by a reduction of the size of the α/β colonies and a decrease in the α-Ti lath thickness, thereby reducing the free path for the dislocation motion. As a result, the strength of the material increases while its ductility decreases.

To quantitatively assess the contribution of grain boundary strengthening to the overall increase in yield strength, a modified Hall–Petch relation was used, taking into account the specific features of grain structure morphology. The calculations considered the equivalent size of β-Ti columnar grains (L), the average size of β-Ti equiaxed grains (D), the thickness of α-Ti laths (b), and the corresponding volume fractions of each grain type [15,16] . The Hall–Petch relation, which account for both columnar and equiaxed β-Ti grains, is represented by the following Eq. (4):

$$\Delta\sigma_{GB} = \sigma_0 + K(L)^{-1/2} \cdot V_{\beta col.} + KD^{-1/2} \cdot V_{\beta eq.} + Kb^{-1/2}, \qquad (4)$$

where K is the Hall-Petch coefficient (K = 0.23 MPa·m$^{1/2}$) [16]; L is the equivalent size of β-Ti columnar grains; $V_{\beta col.}$ is the volume fraction of columnar grains; D is the average size of equiaxed β-Ti grains; $V_{\beta eq.}$ is the volume fraction of equiaxed grains; b is the thickness of α-Ti laths. The calculation results show that its contribution to grain boundary strengthening varies significantly depending on the microstructure morphology formed at different iron contents. When alloyed with 1.7, 2.5, and 7.5 wt.% Fe, the contribution of grain boundary strengthening is 432, 524, and 139 MPa, respectively (Table 2).

The contribution of solid solution strengthening upon alloying Ti4Al3V with iron was estimated using the Eq. (5) [17]:

$$\Delta\sigma_{SS} = K_0\sigma_0 + K_{Al}C_{Al} + K_V C_V + K_{Fe}C_{Fe}, \qquad (5)$$

In this study, the strengthening coefficient K_0 for α-Ti, equal to 1.23, was applied in the calculations for Ti4Al3V-1.7Fe and Ti4Al3V-2.5Fe alloys. For the Ti4Al3V-7.5Fe alloy, which is predominantly β phase, the strengthening coefficient for β-Ti, equal to 1.18 [18], was employed. The coefficients K_{Al}, K_V, and K_{Fe} correspond to the increase in the yield strength per 1 wt.% addition of the respective alloying elements and are equal to 60 MPa, 20 MPa, and 46 MPa, respectively. The variables C_{Al}, C_V, and C_{Fe} denote the concentrations (wt.%) of the corresponding alloying elements in the alloy. Since Al and V are already present as alloying elements in the two-phase Ti4Al3V alloy, the solid solution strengthening was evaluated taking into account the contributions of K_{Fe} and C_{Fe}. Analysis of the results indicates that the contribution of solid solution strengthening to the yield strength increment of Ti4Al3V-1.7Fe, Ti4Al3V-2.5Fe, and Ti4Al3V-7.5Fe alloys is 186, 234, and 456 MPa, respectively (Table 2).

Analysis of transmission electron microscopy results demonstrated that the contribution of dislocation hardening to the total increase in the yield strength for these alloys is less than 5%, which is attributed to the low dislocation density formed during alloy solidification (Fig. 2). Consequently,

Table 2. Yield strength, tensile strength, and contributions of individual strengthening mechanisms in Ti4Al3V alloy doped with various Fe contents.

Sample	Experiment		Calculation			
	YS, MPa	UTS, MPa	$\Delta\sigma_{GB}$, MPa	$\Delta\sigma_{SS}$, MPa	$\Delta\sigma_{\omega}$, MPa	$\Delta\sigma_{YS}$, MPa
Ti4Al3V-1.7Fe	724 ± 40	785 ± 39	432	186	0	747
Ti4Al3V-2.5Fe	859 ± 42	927 ± 45	524	234	0	887
Ti4Al3V-7.5Fe	820 ± 57	820 ± 57	139	456	107	831

this strengthening mechanism was excluded from the overall strengthening calculations of Ti4Al3V-Fe alloys.

According to the equilibrium phase diagram of the Ti-Fe system, intermetallic compounds such as TiFe and Ti_2Fe form when the iron content exceeds 15 wt.% under certain temperature conditions [19]. In the Ti4Al3V alloy investigated in this study, with the iron content ranging from 1.7 to 7.5 wt.% Fe, i. e. it is significantly below the threshold for the formation of intermetallic phases. Transmission electron microscopy and EDS analysis further confirm the absence of either TiFe or Ti_2Fe phases; therefore, there is no additional contribution to the yield strength due to dispersion strengthening (Table 2). The metastable ω-Ti phase is a special type of martensitic phase that forms in β-stabilized titanium alloys. Its formation occurs in a diffusionless manner through a shear mechanism characteristic of martensitic transformation [20]. Internal stresses arising from lattice mismatches at the ω/β phase boundaries play a key role in strengthening titanium alloys by promoting dislocation pinning and the formation of loops around coherent ω-precipitates. These features hinder dislocation motion, increasing hardness but reducing ductility. When the ω-phase volume fraction exceeds ≈5–7%, a significant decline in deformation properties is observed [21].

In additive manufacturing, including the electron beam additive manufacturing, the deposited layers inevitably undergo repeated reheating. This creates favorable conditions for isothermal precipitation of the ω-Ti in titanium alloys [22]. The probability of ω-Ti precipitation within the β-Ti grains also increases due to the relatively low cooling rates of the molten pool, which is typical for WEBAM. It was established that in the Ti4Al3V-7.5Fe alloy, the ω-Ti forms as equiaxed precipitates with a size of 4.36±1.22 nm, which is consistent with the data obtained by TEM and XRD (Fig. 2i–k, Fig. 4a,b). The quantitative evaluation of the contribution of nanoscale ω-Ti precipitates formed during iron alloying of Ti4Al3V, to the increase in the yield strength can be performed using the following equation [23]:

$$\Delta\sigma_{\omega} = 2.83\gamma_{\omega}^{3/2} G_S^{-1/2} b^{-2} r_{\omega}^{1/2} f_{\omega}^{1/2}, \qquad (6)$$

where γ_{ω} is the anti-phase boundary energy of ω-Ti (0.1 J/m^2), G_S is the shear modulus of ω-Ti during dislocation slip along $<110>_{\beta}$ (15 GPa), b is the Burgers vector of bcc-Ti (0.28 nm), r_{ω} and f_{ω} represent the average radius and volume fraction of ω-Ti precipitates equal to 4.36 nm and 3%, respectively. Analysis of the results shows that the contribution of nanoscale ω-Ti precipitates to the hardening of Ti4Al3V-7.5Fe is 107 MPa. It has been experimentally established that the average yield strength of Ti4Al3V alloy doped with 1.7, 2.5, and 7.5 wt.% Fe is 724±40, 859±42, and 820±57 MPa, respectively. These values are in good agreement with the calculated yield strengths for Ti4Al3V-1.7Fe (747 MPa), Ti4Al3V-2.5Fe (887 MPa), and Ti4Al3V-7.5Fe (831 MPa) alloys.

Figure 6 shows the dependency of the contributions of grain boundary and solid solution strengthening on the iron content in the Ti4Al3V alloy. Figure 6 also presents the values of $\Delta\sigma_{GB}$ and $\Delta\sigma_{SS}$ for Ti4Al3V alloys with 3.3 and 4.7 wt.% Fe, produced by laser wire deposition [6] microstructure, and mechanical properties (including hardness and strength.

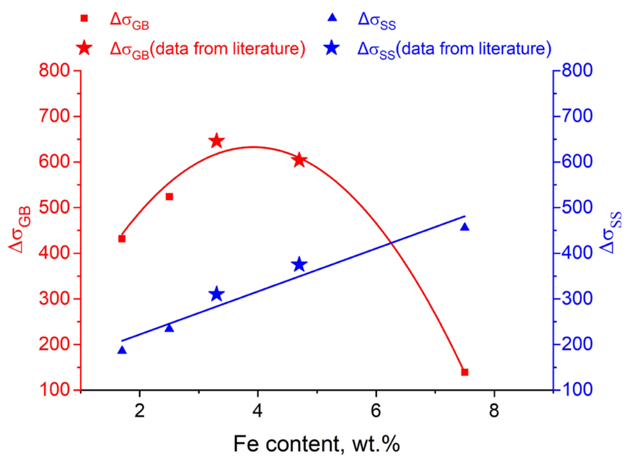

Fig. 6. (Color online) Evaluation of the contributions of grain boundary and solid solution strengthening mechanisms to the hardening of the Ti4Al3V-Fe alloy.

Analysis of the data shows that, for Ti4Al3V alloy doped with iron in the range of 1.7–3.3 wt.%, grain boundary strengthening is the dominant strengthening mechanism, resulting from the refinement of both prior β-Ti grains and α-Ti laths.

The contribution of grain boundary strengthening to the increase in the yield strength of the Ti4Al3V-7.5Fe alloy is only 19%, which is significantly lower than that observed in alloys with a lower iron content. This reduction is attributed to changes in the microstructural morphology, accompanied by a decrease in the number of grain boundaries. The high volume fraction of the β phase (92%) leads to a decrease in the fraction of α-Ti laths, which, in turn, reduces the density of grain boundaries and α/β colonies, thereby weakening the effect of the Hall-Petch strengthening mechanism. Consequently, grain boundary strengthening makes a relatively minor contribution to the overall yield strength increase in the Ti4Al3V-7.5Fe alloy. Therefore, at an iron content of 7.5 wt.%, the primary strengthening mechanism is solid solution strengthening due to the dissolution of iron in β-Ti.

5. Conclusions

The paper discusses the strengthening mechanisms of Ti-Al-V-Fe alloys across a broad range of iron concentrations. Both computational and experimental results confirm that the addition of iron to the Ti4Al3V titanium alloy significantly influences the grain structure morphology and phase composition, which in turn determines the contribution of each strengthening mechanism to the increase in the yield strength. It was found that increasing the iron content from 1.7 to 7.5 wt.% in the Ti4Al3V alloy leads to a refinement of the prior β-Ti grains and transforms the microstructure from columnar-equiaxed to fully equiaxed. Experimental data show that increasing the iron content from 1.7 to 2.5 wt.% results in a substantial increase in the tensile yield strength by 24% and 47%, respectively, compared to the Ti4Al3V alloy without iron addition.

Thus, Ti4Al3V alloys with 1.7 and 2.5 wt.% Fe offer an optimal balance of strength and ductility due to grain refinement and solid-solution strengthening from Fe in the β-Ti phase. Increasing the Fe content to 7.5 wt.% further enhances strength but reduces ductility, which should be considered in design. Nevertheless, such alloys show promising tribological performance, making them suitable for wear-intensive applications.

This reduction is attributed to the formation of prior equiaxed β-Ti grains with ω-Ti precipitates, instead of the typical α/β lath microstructure. Thus, knowing the iron concentration allows for accurate prediction of the contribution of each strengthening mechanism to the overall alloy hardening, which is crucial for designing alloys with tailored properties.

References

1. M. Peters, J. Kumpfert, C.H. Ward, C. Leyens, Titanium alloys for aerospace applications, Adv. Eng. Mater. 5 (2003) 419–427.
2. E. Uhlmann, R. Kersting, T.B. Klein, M.F. Cruz, A.V. Borille, Additive manufacturing of titanium alloy for aircraft components, Procedia CIRP 35 (2015) 55–60.
3. J.C. Williams, R.R. Boyer, Opportunities and issues in the application of titanium alloys for aerospace components, Metals 10 (2020) 705.
4. T. DebRoy, H.L. Wei, J.S. Zuback, T. Mukherjee, J.W. Elmer, J.O. Milewski, A.M. Beese, A. Wilson-Heid, A. De, W. Zhang, Additive manufacturing of metallic components — process, structure and properties, Prog. Mater. Sci. 92 (2018) 112–224.
5. Y. Liu, W. Jiang, Z. Chen, Q. Xu, Z. Zhang, J. He, Optimization of processing parameters and microstructure evolution of (TiB+La_2O_3)/Ti6Al4V manufactured by laser melting deposition, J. Mater. Res. Technol. 24 (2023) 8086–8097.
6. X. Wang, L.J. Zhang, J. Ning, S. Li, L.L. Zhang, J. Long, W. Ma, Fe element promotes the transformation from columnar to equiaxed grains and the formation of ultrafine microstructure of Ti-6Al-4V alloy by laser wire deposition, Addit. Manuf. 48 (2021) 102442.
7. A.V. Nikolaeva, A.P. Zykova, V.V. Shmakov, S.Y. Tarasov, Evaluation of contributions of hardening mechanisms to the yield strength of Ti6Al4V-Cu alloys produced by wire electron beam additive manufacturing, Lett. Mater. 14 (2024) 204–209.
8. Z. Chen, Y. Peng, X. Zhang, J. Fan, S. He, J. Kong, K. Wang, Influence of trace silicon addition on microstructure and properties of Ti6Al4V fabricated by wire arc additive manufacturing, J. Mater. Res. Technol. 23 (2023) 1347–1359.
9. H. Liu, M. Fang, Y. Han, G. Huang, Z. Sun, L. Zhang, W. Lu, Achieving strength-ductility combination and anisotropy elimination in additively manufactured TiB/Ti6Al4V by in-situ synthesized network architecture with fine grains, Compos. Part B Eng. 262 (2023) 110822.
10. C. Guo, G. Dai, J. Niu, Y. Guo, Z. Sun, H. Chang, Q. Zhang, Fe nanoparticles modified pure Ti alloy on microstructure evolution and fine crystallization mechanism fabricated by additive manufacturing, J. Mater. Res. Technol. 26 (2023) 5860–5872.
11. R.M. Jones, Mechanics of Composite Materials, second ed, CRC Press, Boca Raton, 2018, 519 p.
12. P. Luo, D.T. McDonald, W. Xu, S. Palanisamy, M.S. Dargusch, K. Xia, A modified Hall–Petch relationship in ultrafine-grained titanium recycled from chips by equal channel angular pressing, Scr. Mater. 66 (2012) 785–788.
13. G.S. Dyakonov, S. Mironov, I.P. Semenova, R.Z. Valiev, Strengthening mechanisms and super-strength of severely deformed titanium, in: Micro and Nano Technologies, Nanocrystalline Titanium, 2019, pp. 123–143.
14. P. Luo, Analysis of microstructure and its effect on yield strength of pure alpha-titanium consolidated by equal channel angular pressing, Mater. Trans. 59 (2018) 1161–1165.
15. M.A. Easton, M. Qian, A. Prasad, D.H. StJohn, Recent advances in grain refinement of light metals and alloys, Curr. Opin. Solid State Mater. Sci. 20 (2016) 13–24.
16. Y. Chong, G. Deng, S. Gao, J. Yi, A. Shibata, N. Tsuji, Yielding nature and Hall–Petch relationships in Ti-6Al-4V alloy with fully equiaxed and bimodal microstructures, Scr. Mater. 172 (2019) 77–82.
17. S.L. Semiatin, V. Seetharaman, I. Weiss, Flow behavior and globularization kinetics during hot working of Ti-6Al-4V with a colony alpha microstructure, Mater. Sci. Eng. A. 263 (1999) 257–271.
18. K. Zhou, P. Han, W. Wang, H. Yang, X. Guo, J. Hou, Y. Zhang, K. Qiao, F. Qiang, K. Wang, Microstructure and tensile properties of a large-scale Ti-4.5Al-3V-2Mo-2Fe alloy plate with ultrafine grains prepared by multi-pass friction stir processing, Mater. Today Commun. 45 (2025) 112324.
19. J.H. Han, G.A. Song, J.M. Park, J.K. Lee, S. Yi, D.H. Kim, K.B. Kim, Microstructural modulation of Ti-Fe-V ultrafine eutectic alloys with enhanced mechanical properties, J. Alloys Compd. 491 (2010) 178–181.
20. H. Azizi, H. Zurob, B. Bose, S.R. Ghiaasiaan, X. Wang, S. Coulson, V. Duz, A.B. Phillion, Additive manufacturing of a novel Ti-Al-V-Fe alloy using selective laser melting, Addit. Manuf. 21 (2018) 529–535.
21. K. Tsuchiya, S. Emura, X. Ji, I. Gutierrez, T. Hara, Plastic deformation of beta-Ti-Mo alloys with isothermal omega phase, MATEC Web Conf. 321 (2020) 11087.
22. C. Guo, J. Xia, G. Dai, Y. Guo, Z. Sun, H. Chang, Q. Zhang, Enhanced mechanical properties and refined microstructure induced by micron Fe for additive manufactured Ti-Fe alloys, J. Alloys Compd. 1033 (2025) 181144.
23. Y. Liu, L. Xu, C. Qiu, Development of an additively manufactured metastable beta titanium alloy with a fully equiaxed grain structure and ultrahigh yield strength, Addit. Manuf. 60 (2022) 103208.